Hindawi Publishing Corporation
Journal of Electrical and Computer Engineering
Volume 2014, Article ID 631867, 11 pages
http://dx.doi.org/10.1155/2014/631867

Research Article

Performance of 2–3.6 GHz Five-Port/Three-Phase Demodulators with Baseband Analog I/Q Regeneration Circuit in Direct-Conversion Receivers

Kaissoine Abdou,[1] Antoine Khy,[1] Kais Mabrouk,[2] and Bernard Huyart[1]

[1] *Communications and Electronics Department, TELECOM ParisTech, 46 rue Barrault, 75013 Paris, France*
[2] *Laboratoire de Recherche et d'Innovation Technologique, Ecole Polytechnique de Sousse, rue Khalifa Karoui Sahloul, 4000 Sousse, Tunisia*

Correspondence should be addressed to Antoine Khy; antoine.khy@telecom-paristech.fr

Received 4 October 2013; Revised 24 December 2013; Accepted 26 December 2013; Published 20 February 2014

Academic Editor: Serioja Tatu

A comparison between performance of a five-port demodulator (FPD) and a three-phase demodulator (TPD) with both architectures connected to a so-called baseband I/Q regeneration circuit is carried out. In order to compare these two receivers to a classical architecture, the performance of an I/Q demodulator (IQD) is also presented. Measured results show the superiority of TPD and IQD over FPD in terms of residual DC offsets and 2nd order intermodulation distortion (IMD2) products, noise figure (NF), and sensitivity due to the use of active balanced mixers instead of diode power detectors. Lastly, demodulation of three noncontiguous RF carriers shows the stronger potential of the three-phase demodulator (TPD) for applications in future long term evolution-advanced (LTE-A) receivers through EVM and constellation diagram measurements.

1. Introduction

When it was first introduced in the beginning of the 70's, the six-port technique was originally used in metrology to accurately measure reflection coefficients of complex impedances [1] like a vectorial network analyzer (VNA). Since then, the field of applications of six-port systems has been extended to measurement of direction of arrival (DoA) of multiple signals [2, 3], phase/frequency discriminator for automobile radars [4, 5], microwave and millimeter-wave sensing [6], and demodulators in direct-conversion receivers [7–20]. The six-port technique is based on an RF circuit with 2 inputs and 4 outputs that performs the linear combination of the 2 input signals, 4 power detectors connected to each output of the RF circuit for quadratic detection, 4 analog-to-digital converters (ADCs), and a digital calibration procedure. The main advantage of the six-port technique is due to the inherent redundancy of the output data that allows alleviating the performance of the RF components of the circuit. On the other hand, the downside of this lies in the use of 4 ADCs at the outputs of the system. However, in direct-conversion receiver applications, the number of ADCs can be reduced to 3 by using the so-called five-port technique [21–26]. In this particular case, the power level of the local oscillator (LO) is supposed to be constant or prone to very small variations, which accordingly permits the suppression of one ADC. In order to further reduce the number of ADCs to only 2 likewise conventional I/Q architectures, the 3 outputs of the five-port circuit have to be designed so that one of them is an amplitude and phase symmetry axis in relation to the two others [26–28]. When these two conditions are fulfilled, a single analog OP-amp circuit can be connected to the 3 outputs of the five-port to perform basic operations (sum and difference) between them, resulting in two 90° quadrature I and Q output components of the demodulated RF signal. For this reason, we call this analog OP-amp circuit a baseband I/Q regeneration circuit [26]. Other valuable benefits of the use of this circuit are DC offsets suppression and 2nd order intermodulation distortion (IMD2) cancellation, which are serious issues in direct-conversion receivers [29].

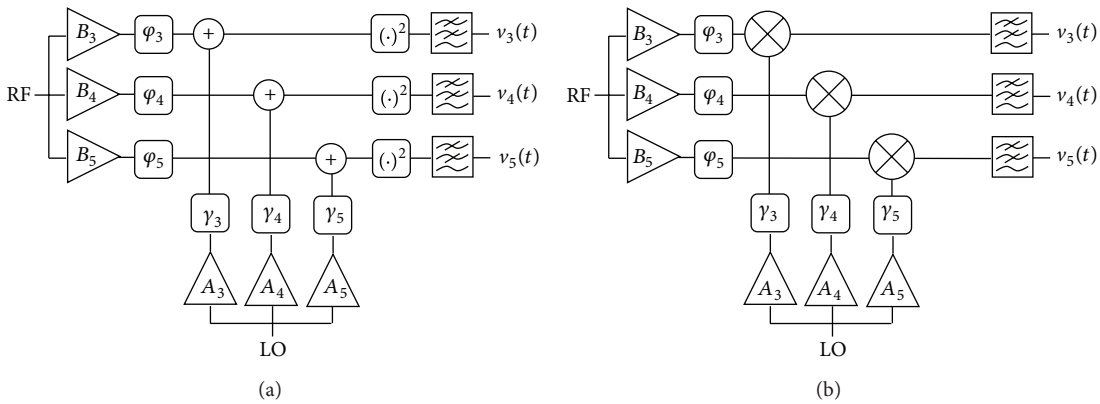

Figure 1: General model of the (a) FPD and (b) TPD.

Lastly, it should be pointed out that the use of the I/Q regeneration circuit allows to avoid the tedious calibration procedure mentioned above for a five-port circuit alone [21]. However, in practice the two outputs of the I/Q regeneration circuit are two scaled versions of the actual I and Q components, showing amplitude and phase mismatch. Thus, the actual I and Q values are determined by means of simple amplitude/phase equalization. In [26], a 2.1 GHz microstrip ring-based five-port system used with the I/Q regeneration circuit exhibits $90 \pm 5^{\circ}$ phase shifted I and Q components over more than 2 octaves, 10 dB DC offsets suppression, and up to 23 dB IMD2 rejection compared to microstrip five-port circuit alone. However, the main drawback of five- or six-port architectures used in direct-conversion receivers is their low sensitivity due to the very high conversion loss (30–40 dB) of diode power detectors. In [30], for a 2.1 GHz microstrip five-port circuit that uses Agilent HSMS-2850 diodes for detection, measured conversion loss is 39 dB and noise figure is 36 dB. Simulation results in [12] show that conversion loss can be reduced to 16 dB with the use of Agilent HSCH-9161 diodes. In this paper, the FPD uses tunnel diodes instead of Schottky diodes that exhibit less than 11 dB conversion loss, which still remains unacceptable. To improve sensitivity of five- or six-port circuits, mixers can be used instead of diodes since they show lower conversion loss (even conversion gain for active mixers) and lower noise figure and generate less DC offsets and IMD2 products. Obviously, since mixers are three-port devices, the RF circuit that performs the linear combination of the RF and LO signals has to be slightly modified compared to the case of two-port power detectors. For this reason, the naming "three-phase demodulator" (TPD) is used for this type of architecture including mixers while the "five-port demodulator" (FPD) term is dedicated to architectures with power detectors, only.

In this paper, the performances of an FPD and a TPD both connected to the baseband I/Q regeneration circuit discussed above are studied and compared to those obtained with a classical I/Q demodulator (IQD). These 3 receivers are dedicated to long term evolution-advanced (LTE-A) applications and operate between 2 GHz and 3.6 GHz. While the spectrum allocated to future LTE-A systems is expected to span from 700 MHz to 3.6 GHz, our study was limited to the 2–3.6 GHz frequency range due to the limited bandwidth of the 3-way power dividers used in the implemented FPD and TPD. First, the operating principles of the FPD, TPD and the I/Q regeneration circuit are explained and the implementation of the 2 demodulators is presented. Then, experimental results are presented for I/Q amplitude/phase imbalance, DC offsets and IMD2 products suppression, noise figure, and sensitivity for each architecture. Also, baseband spectrum of three noncontiguous RF signals after demodulation is shown as well as error vector magnitude (EVM) measurements and constellation diagrams. These results demonstrate the superiority of the TPD architecture in overall performance except for residual DC offsets that are higher in TPD than in IQD. To the best of our knowledge, this is the first study dealing with performance comparison between FPD, TPD, and IQD.

2. Five-Port Demodulator (FPD) and Three-Phase Demodulator (TPD) Basic Principles

Figure 1 shows the general models of the FPD and TPD that are used in direct-conversion receiver architectures. The difference between FPD and TPD lies in the active devices used for downconversion, which are detectors and mixers for FPD and TPD, respectively. The circuits have 2 inputs for LO and RF signals and 3 low frequency outputs $v_3(t)$, $v_4(t)$, and $v_5(t)$. After LO and RF signals are both split by 3-way power dividers with different attenuation coefficients A_i and B_i and phase shifts γ_i, φ_i ($i = 3, 4, 5$), the signals are combined together by means of adders. Then, square-law devices perform envelope detection as well as downconversion, low-pass filters suppress any high frequency components, and lastly, three ADCs digitize the output voltages $v_3(t)$, $v_4(t)$, and $v_5(t)$. In the case of the TPD, the adders and envelope detectors are replaced by mixers that multiply LO and RF signals [23, 28]. Although, devices used for downconversion differ in the FPD and TPD, the basic operating principle is the same for both. In depth analysis with equations derivations can be found in [21, 26, 27].

It can be shown that the 3 low frequency voltages of the FPD or TPD can be expressed as follows:

$$v_i(t) = \frac{K_i}{2}A_i^2V_{\mathrm{LO}}^2 + \frac{K_i}{2}B_i^2\left[I^2(t) + Q^2(t)\right] + K_iV_{\mathrm{LO}}A_iB_i \times \left[\cos(\gamma_i - \varphi_i)\, I(t) + \sin(\gamma_i - \varphi_i)\, Q(t)\right] \quad i = \{3, 4, 5\}, \tag{1}$$

where K_i is the second-order coefficient of the diode transfer characteristic (resp., conversion loss of the mixer) at port i in the case of the FPD (resp., TPD) while $I(t)$ and $Q(t)$ are the in-phase and quadrature-phase components of the input modulated RF signal. The first term in (1), that is a DC component, is due to LO signal self-mixing. It is the main contributor to DC offsets. The second term, which comprises a DC and low frequency time variant components, results from self-mixing of the RF signal. This low frequency component is the IMD2 product. As for the last term, it contains the desired actual $I(t)$ and $Q(t)$ components. Accordingly, (1) can be rewritten as follows:

$$v_i(t) = \mathrm{DC}_i + \mathrm{IMD2}_i(t) + K_iV_{\mathrm{LO}}A_iB_i\left[\cos(\Phi_i)\, I(t) + \sin(\Phi_i)\, Q(t)\right] \quad i = \{3, 4, 5\}, \tag{2}$$

where DC_i is the sum of the DC components due to LO and RF signals self-mixing; $\mathrm{IMD2}_i(t)$ is the low frequency time variant component due to 2nd order nonlinearity and $\Phi_i = \gamma_i - \varphi_i$.

3. Baseband Analog I/Q Regeneration Circuit

As mentioned before, if one of the 3 low frequency voltages $v_i(t)$ is an amplitude and phase symmetry axis in relation to the 2 others, the number of ADCs in Figure 1 can be reduced to only two by adding a single I/Q regeneration circuit at the three outputs of the FPD or TPD. If we arbitrarily choose $v_4(t)$ as the symmetry axis, these 2 conditions can be stated as follows:

(1) amplitude symmetry condition:

$$A_3 = A_5 = A, \qquad B_3 = B_5 = B, \qquad K_3 = K_5 = K, \tag{3}$$

(2) phase symmetry condition:

$$\phi_3 = C_0 + \alpha, \qquad \phi_4 = C_0, \qquad \phi_5 = C_0 - \alpha, \tag{4}$$

where C_0 is a phase shift of $v_4(t)$ whose effect is a rotation of the I-Q phase diagram of an angle equal to C_0. For simplicity, we will consider that $C_0 = 0$.

Now, if the amplitude symmetry condition is extended to $v_4(t)$, that is,

$$A_3 = A_4 = A_5 = A, \qquad B_3 = B_4 = B_5 = B, \qquad K_3 = K_4 = K_5 = K, \tag{5}$$

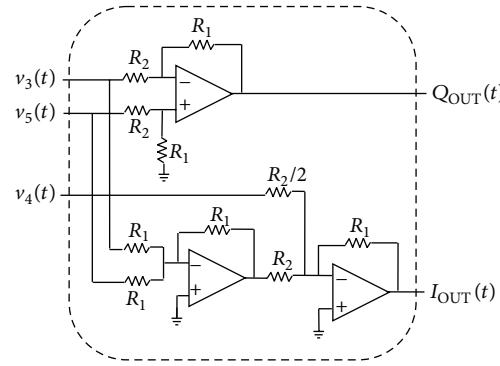

Figure 2: Architecture of the baseband analog I/Q regeneration circuit.

then, it can be shown that the actual $I(t)$ and $Q(t)$ components are [26, 27]

$$I(t) = \mu_I\left[-v_3(t) + 2v_4(t) - v_5(t)\right] = \mu_I I_{\mathrm{OUT}}(t), \qquad Q(t) = \mu_Q\left[v_3(t) - v_5(t)\right] = \mu_Q Q_{\mathrm{OUT}}(t) \tag{6}$$

with

$$\mu_I = \frac{1}{\left\{2KV_{\mathrm{LO}}AB\left[1 - \cos(\alpha)\right]\right\}}, \qquad \mu_Q = \tan\left(\frac{\alpha}{2}\right)\cdot\mu_I. \tag{7}$$

The I/Q regeneration circuit whose architecture is shown in Figure 2 realizes the sums and differences of the output voltages $v_i(t)$ to compute $I_{\mathrm{OUT}}(t)$ and $Q_{\mathrm{OUT}}(t)$ in (6). These are scaled versions of the actual $I(t)$ and $Q(t)$ components, so an equalization procedure is needed.

However, it is shown in [26] that the quadrature of $I(t)$ and $Q(t)$ is ensured as long as the two symmetry conditions stated in (3) and (4) remain fulfilled, independently of the value of α, so that no phase compensation has to be applied. On the other hand, the amplitude of $I(t)$ and $Q(t)$ is function of α and they differ from each other except when $\alpha = 90^\circ$ and (5) are fulfilled. In this particular case, $I_{\mathrm{OUT}}(t)$ and $Q_{\mathrm{OUT}}(t)$ have the same amplitude and since quadrature is always satisfied, the actual $I(t)$ and $Q(t)$ components are directly recovered from $I_{\mathrm{OUT}}(t)$ and $Q_{\mathrm{OUT}}(t)$ without any amplitude/phase compensation, and therefore, no equalization procedure is required if the transmitter is directly connected to the receiver. However, in a real communication link, equalization is still needed due to the degradation of RF propagation channel. Furthermore, amplitude symmetry condition in (5) allows the I/Q regeneration circuit to suppress DC offsets and IMD2 products in both I and Q paths. Indeed, if the 3 paths of the FPD or TPD are perfectly identical, the DC_i and $\mathrm{IMD2}_i(t)$ in (2) are canceled when $v_i(t)$ is substituted into (6). The Analog Devices AD8056A OP-amp circuit was used in the fabricated prototype and the values of the resistors were chosen in order to obtain a unity voltage gain in each of the I and Q paths, as in [26].

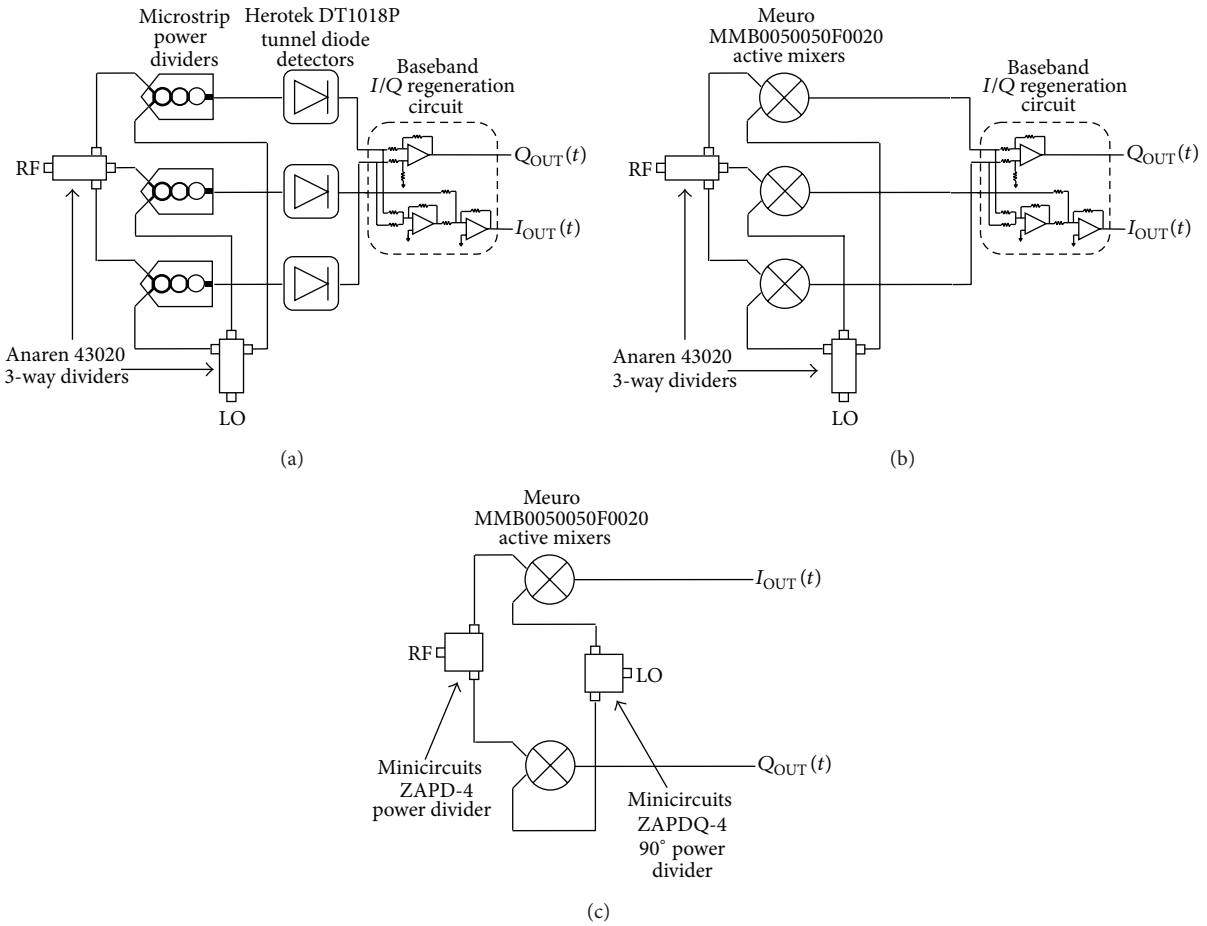

Figure 3: Schematic of (a) FPD and (b) TPD architectures with baseband I/Q regeneration circuit (c) IQD.

4. Implementation of Five-Port (FPD), Three-Phase (TPD), and I/Q Demodulators (IQD)

Figure 3 shows a schematic of FPD and TPD with baseband analog OP-amp circuit for I/Q regeneration as well as IQD architecture. For FPD and TPD, RF and LO signals are split by means of Anaren 43020 3-way power dividers showing insertion loss below 0.4 dB in each branch and isolation better than 23 dB between 2 GHz and 3.6 GHz. FPD architecture implies the use of 1 GHz to 4 GHz microstrip power dividers fabricated in our lab on printed circuit boards (PCBs) in order to combine the RF and LO signals to deliver to the power detectors. These are based on Herotek DT1018P tunnel diodes showing tangential signal sensitivity (TSS) of −50 dBm and gain flatness of ±1 dB from 1 GHz to 18 GHz. For the TPD and IQD, the downconversion operation is performed by means of Meuro MMB0050050F0020 active mixers exhibiting 10 dB conversion gain and above 30 dB LO-to-RF isolation from 0.45 GHz to 3.6 GHz.

In the IQD, RF signal is split by a Mini-Circuits ZAPD-4 power divider while LO signal is split and 90° phase shifted by a Mini-Circuits ZAPDQ-4 showing less than 7° offset from 90° ideal quadrature in the 2–3.6 GHz frequency range.

5. Measurement Results

5.1. I/Q Amplitude and Phase Imbalance. First, in order to verify the symmetry properties of the implemented FPD and TPD without I/Q regeneration circuit, amplitude and phase of the three low frequency voltages $v_i(t)$ were measured at the outputs of the two architectures. Two continuous-wave (CW) signals with $\Delta f = 10$ kHz separation were applied to the RF and LO input ports of the circuits. Agilent EXG N5172B and E4432B signal generators were used for this purpose with RF power equal to −25 dBm and LO power level set to 5 dBm while the three output voltages $v_i(t)$ were measured by means of Agilent 54622D oscilloscope. Figure 4 shows the measured output voltage amplitudes for FPD and TPD architectures in the 2–3.6 GHz frequency range.

As expected, the output voltage amplitudes are higher in the case of TPD due to the use of active mixers instead of diode detectors, in FPD. Amplitude balance between output voltages $v_3(t)$, $v_4(t)$, and $v_5(t)$ is better for TPD than FPD, especially for frequencies above 3.2 GHz due to mismatch between diode detectors used in FPD architecture. Indeed, amplitude imbalance for TPD does not exceed 1 dB from 2 GHz to 3.6 GHz showing slight performance degradation between 3 GHz and 3.4 GHz. On the other hand, amplitude

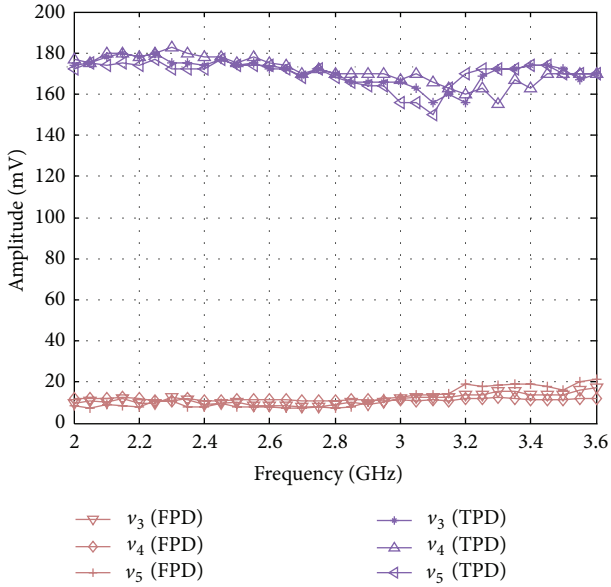

FIGURE 4: Measured output voltage amplitudes for FPD and TPD architectures without I/Q regeneration circuit (P_{LO} = 5 dBm, PRF = −25 dBm, and Δf = 10 kHz).

imbalance for FPD remains below 2.5 dB from 2 GHz to 3.2 GHz but is up to 5 dB from 3.2 GHz to 3.6 GHz. Nevertheless, amplitude imbalance between $v_3(t)$ and $v_5(t)$ is kept below 3.2 dB for FPD. Figure 5 shows phase shift of $v_3(t)$ and $v_5(t)$ with respect to $v_4(t)$ ($\Phi_3 - \Phi_4$ and $\Phi_4 - \Phi_5$) and phase difference between $I(t)$ and $Q(t)$ when the I/Q regeneration circuit is connected to FPD or TPD. For comparison, I/Q phase difference is also plotted for the IQD. Phase imbalance between $v_3(t)$ and $v_5(t)$ with respect to $v_4(t)$ is maintained below 10° and 4° for FPD and TPD, respectively, except between 3 GHz and 3.3 GHz for the latter. In this frequency range, the high discrepancy between $\Phi_3 - \Phi_4$ and $\Phi_4 - \Phi_5$ (up to 25°) originates from mismatch among the active mixers in TPD. This is quite consistent with what is observed in Figure 4 from 3 GHz to 3.4 GHz in terms of components mismatch. As for the absolute value of $\Phi_3 - \Phi_4$ and $\Phi_4 - \Phi_5$, which corresponds to the parameter α introduced in Section 3, it varies approximately from 60° to 125° between 2 GHz and 3.6 GHz for both architectures with ideal value of 90° at the center frequency of 2.8 GHz. This results in 90° ± 10° phase difference between $I_{OUT}(t)$ and $Q_{OUT}(t)$ signals at the output of the I/Q regeneration circuit with perfect 90° quadrature at 2.8 GHz, in accordance with theoretical results. As for the IQD, phase difference between $I(t)$ and $Q(t)$ is 90° ± 7°, showing lower fluctuations around ideal 90° value than FPD and TPD. This is probably due to the fact that the IQD was made with 2 mixers showing better matching between each other among the 3 available mixers.

To demonstrate the sensitivity of the IQD to imbalance between its I and Q paths, the I/Q phase difference is also plotted when the IQD is built with a mixer pair showing higher mismatch. In this configuration, phase difference between $I(t)$ and $Q(t)$ is 100° ± 15°, which features an important degradation of phase quadrature; while, close to ideal 90°, it can still be achieved with the TPD despite the use of one mixer showing poor matching with the two others, hence making evidence of the robustness of the TPD leading to imbalance.

Measured $I_{OUT}(t)$ and $Q_{OUT}(t)$ signal amplitudes at the output of the I/Q regeneration circuit and the IQD are plotted in Figure 6. Amplitude balance better than 1 dB (12% amplitude imbalance) is obtained for the IQD across the 2–3.6 GHz frequency range as mixer pair exhibits good matching. Amplitude imbalance between $I_{OUT}(t)$ and $Q_{OUT}(t)$ signals remains below 1 dB from 2.8 GHz to 3.4 GHz for FPD and from 2.6 GHz to 3 GHz for TPD. Accordingly, very small distortion of the constellation should be observed for these frequencies when a modulated RF signal is applied at the input of the FPD or TPD and equalization procedure could then be avoided. This is consistent with theoretical results in the case of TPD since $\alpha = 90°$ and amplitude symmetry stated in (5) are almost verified between 2.7 GHz and 2.9 GHz but this is quite unexpected in the case of the FPD. Indeed, good $I_{OUT}(t)/Q_{OUT}(t)$ amplitude balance is obtained from 3.2 GHz to 3.4 GHz while α is beyond 110° and high amplitude imbalance is measured between $v_3(t)$, $v_4(t)$, and $v_5(t)$ as shown in Figure 4. This point is still under investigation as correct operation of the I/Q regeneration circuit was verified by applying 3 low frequency voltages at its inputs and measuring quasi null output voltages at I_{OUT} and Q_{OUT} (cf. Figure 2).

5.2. DC Offsets and IMD2 Suppression. As was mentioned in Section 3, the use of the I/Q regeneration circuit allows DC offsets and IMD2 products to be suppressed if voltages $v_3(t)$, $v_4(t)$, and $v_5(t)$ have same amplitude which is stated in (5). In order to verify this property, we measured the ratio between the DC offsets component and the desired signal at the three outputs of the FPD and TPD and then at the outputs of the I/Q regeneration circuit when connected to both architectures. The measurement setup is the same as for the I/Q amplitude and phase imbalance determination; that is, two CW signals with Δf = 10 kHz separation were applied to the circuit with RF and LO power equal to −25 dBm and 5 dBm, respectively, while the output voltages were measured by means of an oscilloscope. From Figure 7, it is clearly evident that the FPD shows much higher DC offsets compared to the TPD and IQD, which was predictable due to the use of double balanced mixers with LO-to-RF isolation above 30 dB in the TPD. When the I/Q regeneration circuit is connected to the FPD, DC offsets suppression is equal to 10 dB on average while in the case of the TPD, it is slightly degraded (6 dB) because of the DC offsets originating from the I/Q regeneration circuit that sum up with the negligible amount of DC offsets generated by the mixers. Nevertheless, residual DC offsets are lower in the TPD compared to the FPD but higher than in IQD since the latter obviously does not make use of any I/Q regeneration circuit.

For the IMD2 products suppression test, we considered a 2.8001 GHz CW desired signal combined with two interfering tones separated from each other by 200 kHz around 2.7 GHz, that is, at 2.7 GHz and 2.7002 GHz, respectively, while LO

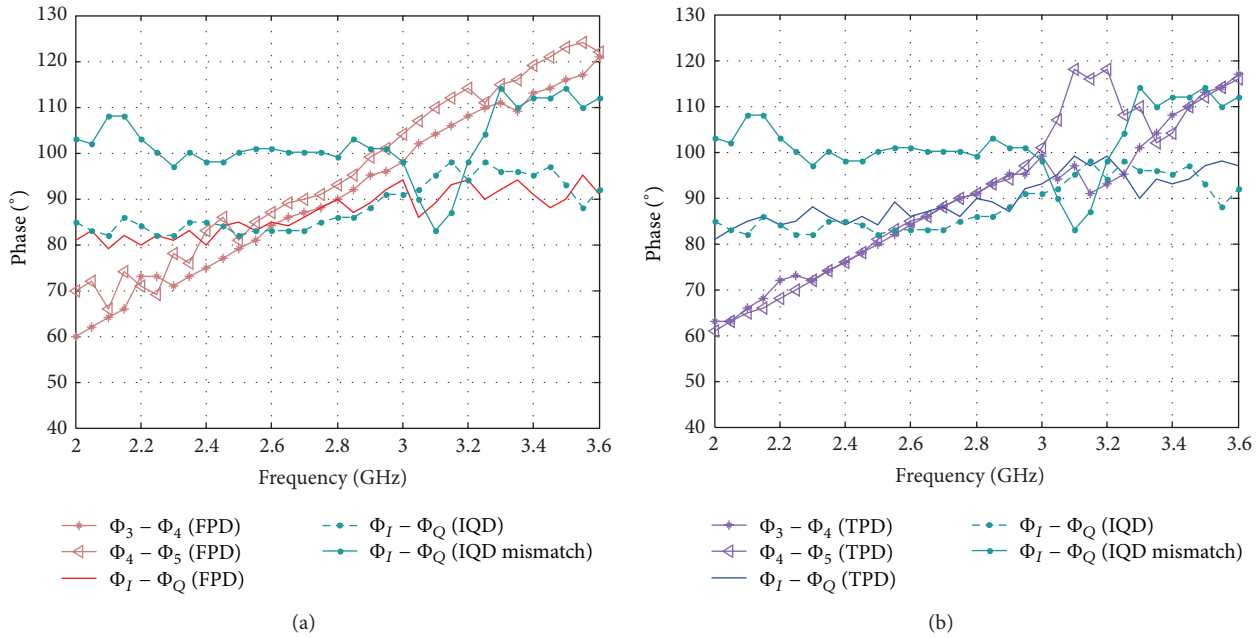

FIGURE 5: Measured phase shift of $v_3(t)$ and $v_5(t)$ with respect to $v_4(t)$ ($\Phi_3 - \Phi_4$, $\Phi_4 - \Phi_5$) and phase difference between $I_{OUT}(t)$ and $Q_{OUT}(t)$ signals for (a) FPD and (b) TPD and comparison with IQD in both cases ($P_{LO} = 5$ dBm, $P_{RF} = -25$ dBm, and $\Delta f = 10$ kHz).

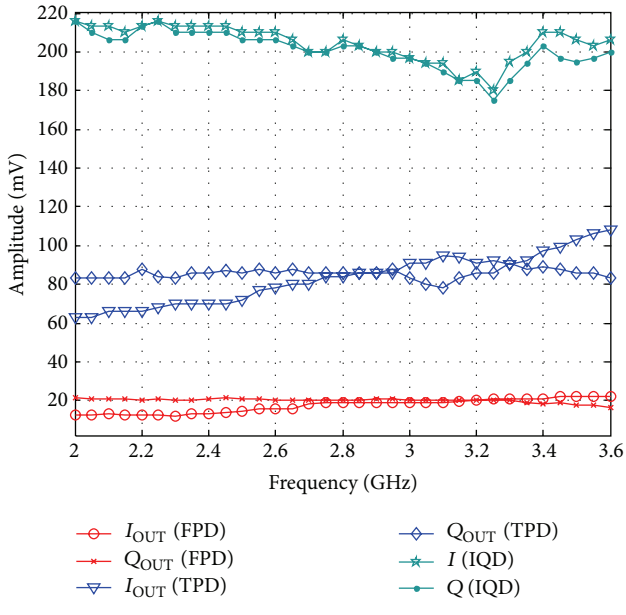

FIGURE 6: Measured amplitudes of $I_{OUT}(t)$ and $Q_{OUT}(t)$ signals at the output of the I/Q regeneration circuit connected to FPD and TPD and for IQD ($P_{LO} = 5$ dBm, $P_{RF} = -25$ dBm, and $\Delta f = 10$ kHz).

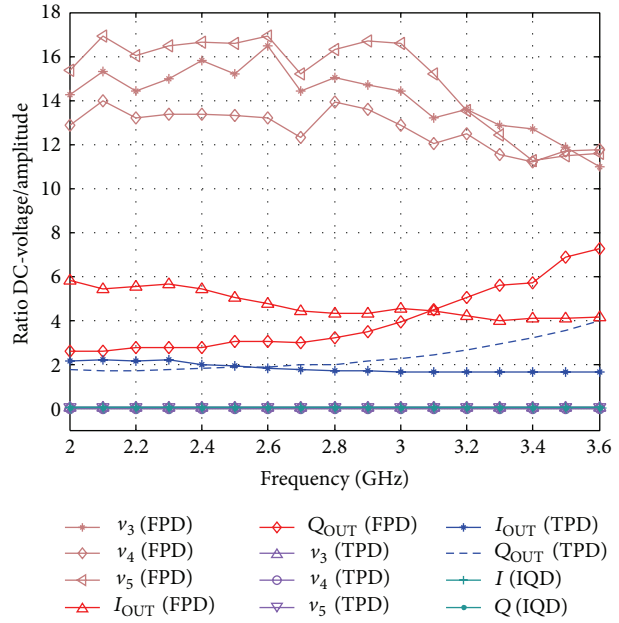

FIGURE 7: Measured DC offsets suppression performance for FPD and TPD and at the outputs of the I/Q regeneration circuit ($P_{LO} = 5$ dBm, $P_{RF} = -25$ dBm, and $\Delta f = 10$ kHz).

frequency was set to 2.8 GHz. Hence, the desired down-converted signal was located at 100 kHz and the IMD2 product component due to mixing of the two interfering tones could be observed at 200 kHz.

In order to evaluate the benefits of the I/Q regeneration circuit, power of the desired useful signal (P_{US}) was compared with power of the IMD2 products (P_{IMD2}) for the FPD and TPD alone and then with the I/Q regeneration circuit connected as the power of the interfering tones (P_{adj}) increases. Figure 8 shows the measured results for $P_{LO} = 5$ dBm, $P_{RF} = -35$ dBm, and P_{adj} varying from -25 dBm to 15 dBm. For the FPD, the use of the I/Q regeneration circuit allows 11–22 dB improvement of the rejection of the IMD2 product in the I output and 10–14 dB in the Q output.

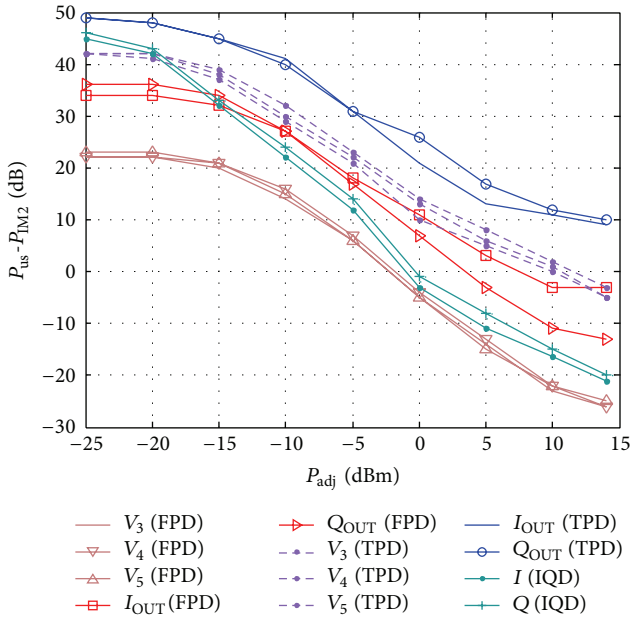

Figure 8: Measured IMD2 products suppression performance versus adjacent channel power P_{adj} of two interfering signals around 2.8 GHz for FPD and TPD and at the outputs of the I/Q regeneration circuit (P_{LO} = 5 dBm and P_{RF} = −35 dBm) connected to both architectures.

In the case of the TPD, the enhancement is 4–12 dB and 6–13 dB in I and Q output, respectively. The moderate improvement in this case compared to FPD is owing to the use of balanced mixers that exhibit less IMD2 products than diode detectors. This feature also explains the higher ratio between P_{US} and P_{IMD2} for TPD than for FPD. Indeed, P_{US}-P_{IMD2} is 10–16 dB and 11–23 dB higher, respectively, in the I and Q output of the TPD compared to FPD. The advantage of the TPD over the IQD is also evident since P_{US}-P_{IMD2} is 4–30 dB better in both I and Q paths. More interesting is the fact that the benefit of the I/Q regeneration circuit is even more noticeable as P_{adj} is increased. Indeed, performance of the IQD collapses with P_{US}-P_{IMD2} < 0 dB when P_{adj} exceeds 0 dBm while for the TPD the ratio P_{US}-P_{IMD2} is still equal to 10 dB even when P_{adj} = 15 dBm.

5.3. Noise Figure and Sensitivity. Noise figure (NF) was determined by the Y-factor method that is the basis of most noise figure measurements whether they are manual or automatically performed by a noise figure analyzer. Using a noise source, this method allows the determination of the internal noise generated within the FPD, TPD (with I/Q regeneration circuit connected), or IQD and therefore, NF or effective input noise temperature of each architecture. With the noise source connected to the RF input of FPD, TPD, or IQD, the output power can be measured when the noise source is turned "on" and "off" and the ratio of these two powers is called the Y-factor. The Rohde & Schwarz FSIQ40 spectrum analyzer was used to measure the Y-factor.

Table 1: Conversion gain (CG), noise figure (NF), and theoretical and measured minimum detectable signal (MDS) for FPD, TPD, and IQD architectures @f = 2.8 GHz for BER = 10^{-3} (1 Msps 0.35 SQRRC-filtered QPSK modulated RF signal with AWGN).

	CG (dB)	NF (dB)	MDS theoretical (dBm)	MDS measurement (dBm)
Power Detector + Combiner	−11	32	—	—
Mixer	10	12	—	—
FPD	−15	34	−63	−50
TPD	12	17	−80	−74
IQD	8	14.6	−82.6	−76.5

Once NF is determined, theoretical sensitivity or minimum detectable signal (MDS) can be calculated by using the following relation for a given signal-to-noise ratio (SNR):

$$\text{MDS (dBm)} = -173.8\left(\frac{\text{dBm}}{\text{Hz}}\right) + 10\log(B) + \text{NF (dB)} + \text{SNR (dB)}, \quad (8)$$

where B is the occupied bandwidth of the RF modulated signal and SNR = E_b/N_0 = 6.8 dB for a quadrature phase shift keying (QPSK) modulation with optimal filtering. E_b is the energy per bit and N_0 is the noise power spectral density. Then, MDS was measured experimentally by considering a 2.8 GHz QPSK modulated RF signal with symbol rate 1 Msps and square-root raised cosine (SQRRC) filtering (roll-off factor = 0.35); that is, B = 1.35 MHz occupied bandwidth. Additive white gaussian noise (AWGN) occupying the same 1.35 MHz bandwidth was superimposed to this signal and MDS was determined as the power of the RF modulated signal corresponding to a given bit-error-rate (BER = 10^{-3}). In practice, RF signal power was increased in order to improve the SNR until BER drops to 10^{-3}. The Agilent E4432B synthesizer was used for RF modulated signal and AWGN generation. A Spectrum MI3033 12-bit data acquisition (DAQ) card was used for sampling of the outputs of the I/Q regeneration circuit connected to FPD and TPD with 8 MHz sampling frequency corresponding to over sampling ratio (OSR) equal to 8. Table 1 compares conversion gain (CG), NF, and theoretical and measured MDS for FPD, TPD, IQD, and power detectors with combiners and mixers. The discrepancy between theoretical and measured MDS values is probably due to quantization noise of the ADCs of the DAQ card. In any case, measured MDS is 24 dB higher in the case of TPD compared to FPD and so the TPD architecture is clearly much better-suited to deal with weak RF signals. On the other hand, IQD shows 2.6 dB better sensitivity than TPD, which was predictable as TPD uses 3 mixers instead of 2 and due to losses in the cables that create the desired phase shifts in TPD. However, the advantage of TPD over IQD lies in its ability to present approximately 20 dB better sensitivity in the presence of strong adjacent interferers (which corresponds to a much realistic situation in practice), as was shown in [31].

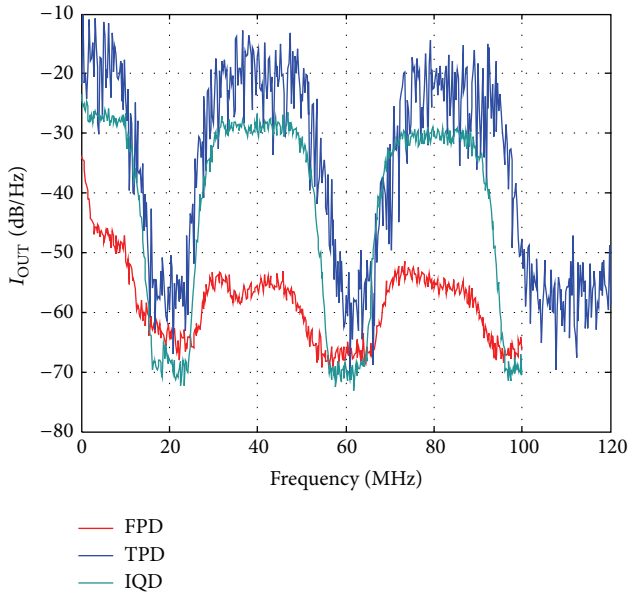

Figure 9: Baseband spectrum at the output of the I/Q regeneration circuit (I path) for FPD, TPD, and IQD after downconversion of three RF carriers @2 GHz, 2.4 GHz, and 2.8 GHz to DC and 40 MHz and 80 MHz.

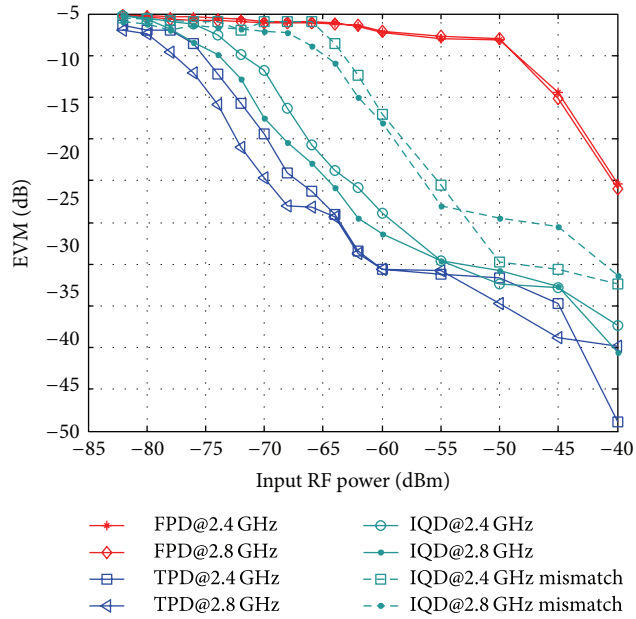

Figure 10: EVM versus RF input power of two 100 kHz 0.35 SQRRC-filtered QPSK modulated carriers @2.4 GHz and 2.8 GHz for FPD, TPD, and IQD.

5.4. RF Carrier Aggregation. FPD and TPD architectures used in conjunction with the I/Q regeneration circuit have strong potential to operate in the presence of several RF noncontiguous aggregated carriers. This feature is particularly interesting for future LTE-advanced (LTE-A) cellular communications. The basic idea is to transpose N discontinuous RF carriers to nonoverlapping frequencies at baseband, that is, DC and N-1 low IF frequencies with a single receiver. In our experiment, three 20 MHz bandwidth SQRRC-filtered (roll-off factor = 0.35) QPSK modulated signals centered at 2 GHz, 2.4 GHz, and 2.8 GHz were down-converted to baseband at DC, 40 MHz, and 80 MHz, respectively, by using a unique FPD or TPD [32, 33]. These signals were synthesized by using Agilent EXG N5172B and two Agilent E8267D vector signal generators with −30 dBm RF power while aggregation was performed with the help of an Anaren 43020 3-way power combiner. The corresponding LO signals, which were delivered by Agilent E4431B, E4432B, and Anritsu MG3691B signal generators were tuned to 2 GHz, 2.36 GHz, and 2.72 GHz with 0 dBm power level. Figure 9 shows the spectrum at the output of the I/Q regeneration circuit for the FPD and TPD in the I path. For comparison, the I path of the IQD is also plotted. The three baseband signals can be clearly identified for each architecture and better sensitivity of TPD and IQD over FPD is also visible due to the use of active mixers instead of power detectors.

Figure 10 shows measurement of error vector magnitude (EVM) versus input power of signal for two 100 kHz bandwidth SQRRC-filtered (roll-off factor = 0.35) QPSK carriers at 2.4 GHz and 2.8 GHz demodulated around 100 kHz and 300 kHz, respectively. The data frame that is received is made of a 16 symbol constant amplitude zero auto correlation (CAZAC) training sequence followed by pseudo random (PN9) useful data.

For a given EVM value of −20 dB (or 10%), the corresponding power level of each of the RF carriers centered at 2.8 GHz is −41 dBm for the FPD, −70 dBm for the TPD, −64.5 dBm for the IQD, and −57 dBm for the IQD showing mismatch between its mixers. Thus, at least 5 dB higher sensitivity of the TPD over IQD is measure, which demonstrates the stronger potential of TPD in the presence of several RF noncontiguous aggregated carriers. Also, sensitivity of the IQD to mismatch is highlighted as 7.5 dB loss in sensitivity that is measured for the IQD with unmatched mixers. Finally, 23–30 dB lower sensitivity of the FPD compared to the two other architectures confirms the results of Table 1 for the MDS. Figure 11 shows the constellation diagrams corresponding to the measurement results plotted in Figure 10 for two −60 dBm QPSK carriers at 2.4 GHz and 2.8 GHz demodulated around 100 kHz and 300 kHz, respectively, for FPD, TPD, and IQD. For the latter, the mixer pair showing good matching was used.

In accordance with measured EVM results for RF power levels as low as −60 dBm, demodulation cannot be effectively performed by the FPD as QPSK constellation shape is not even discernible (EVM = −2.5 dB). Also, the measured symbols at the sampling instants (corresponding to red points in Figure 11) are far from their theoretical location. On the other hand, TPD and IQD architectures successfully recover the received data as the signal trajectories in the $I - Q$ plane clearly show the QPSK constellation diagram and the sampled symbols are located in the vicinity of their respective ideal location. For −60 dBm RF signals, measured EVM is approximately −31 dB for TPD and −25 dB for IQD.

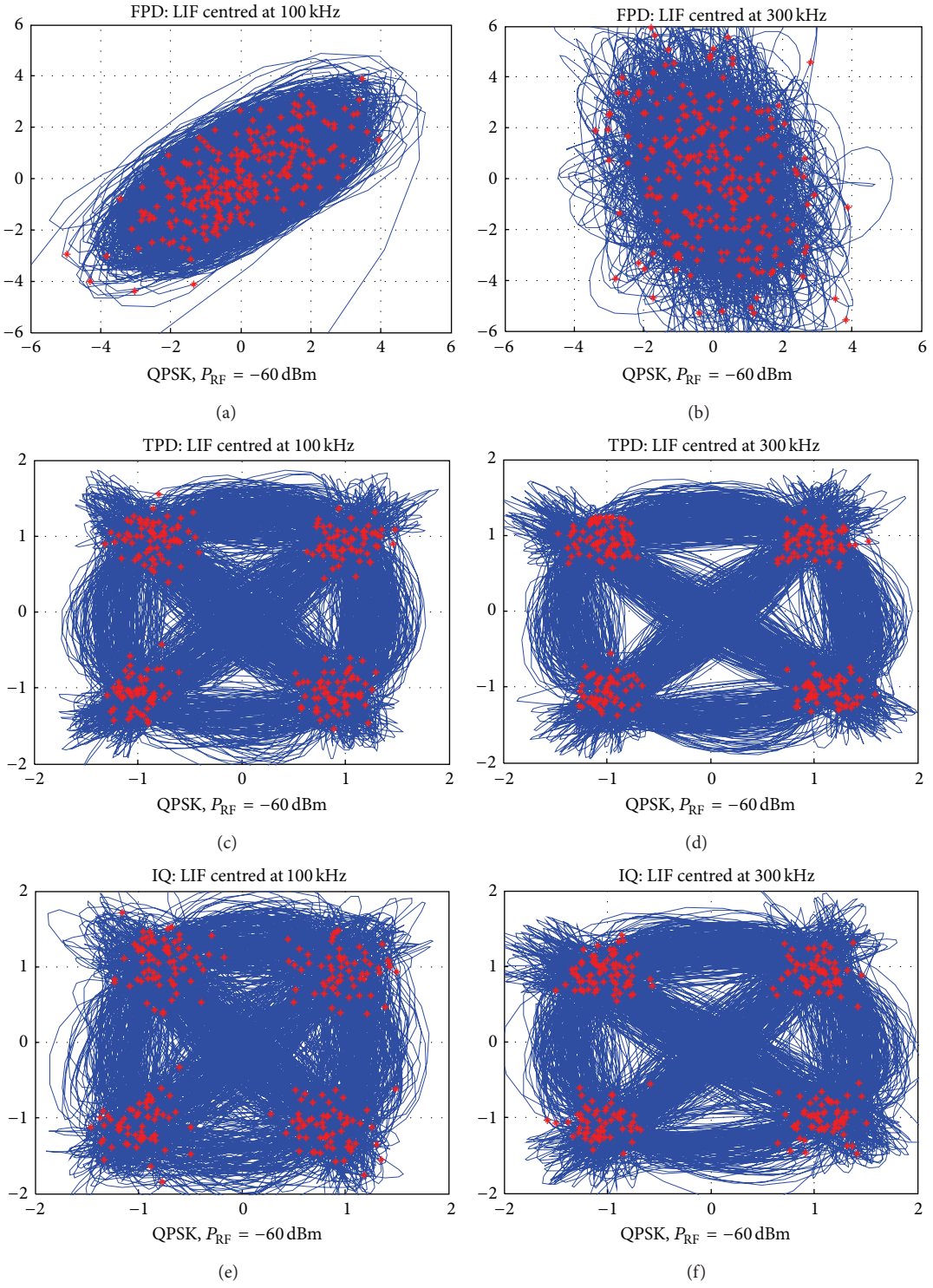

Figure 11: Constellation diagrams corresponding to the demodulation of of two −60 dBm QPSK modulated carriers @2.4 GHz and 2.8 GHz for FPD, TPD, and IQD.

Indeed, a closer look at the constellation diagrams reveals more overshoot of the signal trajectory and scattering of the sampled symbols in the case of IQD (cf. Figure 11(e)) compared to TPD. Table 2 summarizes the performance of FPD, TPD, and IQD architectures.

6. Conclusions

In this paper, a comparison between performance of a five-port demodulator (FPD), a three-phase demodulator (TPD), and an I/Q demodulator (IQD) was carried out.

Table 2: Performance summary of FPD, TPD, and IQD architectures @2.8 GHz.

	FPD	TPD	IQD
CG (dB)	−15	12	8
DC offsets suppression (dB)	−10	6	—
Residual DC/signal (dB)	9.5–17.5	6–12	<−20
IMD2 products suppression (dB)	10–22	4–13	—
Residual IMD2/signal (dB), $P_{RF} = -35$ dBm, $P_{adj} = 15$ dBm	2–13	−10	20
NF (dB)	34	17	14.6
MDS (dBm) (single carrier)	−50	−74	−76.5
P_{RF} @2.8 GHz for EVM = −20 dB (2 aggregated carriers)	−41	−70	−64.5
Power consumption (W)	0	1.8 (12 V, 150 mA)	1.2 (12 V, 100 mA)

FPD and TPD architectures have been measured with a so-called baseband I/Q regeneration circuit connected to their outputs. This circuit not only allows reduction of the number of ADCs from three to two but it also permits DC offsets and IMD2 products suppression. Residual DC offsets and IMD2 products are lower in the case of TPD compared to FPD. Nevertheless, residual DC offsets are higher for TPD compared to IQD due to the use of the I/Q regeneration circuit that creates DC offsets of its own. Also, noise figure (NF) and sensitivity are much better for TPD and IQD. This superiority is not surprising since active balanced mixers show higher performance than diode detectors in every characteristic (conversion gain, DC offsets and IMD2 generation, and NF). Although better sensitivity of IQD is measured in the case of demodulation of a single RF carrier, previous works showed that TPD sensitivity surpasses IQD performance when adjacent interferers are present, which constitutes a much more realistic encountered radio environment in practice. Finally, demodulation of three noncontiguous aggregated RF carriers shows superior performance of the TPD over IQD, through EVM and constellation diagrams measurements. These experimental results tend to present TPD architecture as a potential candidate for future long term evolution (LTE-A) as RF carrier aggregation is one of the main features of this communication standard.

Conflict of Interests

The authors declare that there is no conflict of interests regarding the publication of this paper.

References

[1] G. Engen and C. Hoer, "Application of an arbitrary 6-port junction to power-measurement problems," *IEEE Transactions on Instrumentation and Measurement*, vol. 21, no. 4, pp. 470–474, 1972.

[2] B. Huyart, J.-J. Laurin, R. Bosisio, and D. Roscoe, "Direction-finding antenna system using an integrated six-port circuit," *IEEE Transactions on Antennas and Propagation*, vol. 43, no. 12, pp. 1508–1512, 1995.

[3] B. Laemmle, G. Vinci, L. Maurer, R. Weigel, and A. Koelpin, "A 77 GHz SiGe integrated six-port receiver front-end for angle-of-arrival detection," *IEEE Journal of Solid-State Circuits*, vol. 47, no. 9, pp. 1966–1973, 2012.

[4] J. Li, R. G. Bosisio, and K. Wu, "Collision avoidance radar using six-port phase/frequency discriminator (SPFD)," in *Proceedings of the IEEE National Telesystems Conference*, pp. 55–58, San Diego, Calif, USA, May 1994.

[5] C. G. Miguélez, B. Huyart, E. Bergeault, and L. P. Jallet, "A new automobile radar based on the six-port phase/frequency discriminator," *IEEE Transactions on Vehicular Technology*, vol. 49, no. 4, pp. 1416–1423, 2000.

[6] K. Haddadi and T. Lasri, "60 GHz near-field six-port microscope using a scanning slit probe for subsurface sensing," *IEEE Sensors Journal*, vol. 12, no. 8, pp. 2575–2576, 2012.

[7] J. Li, R. G. Bosisio, and K. Wu, "Computer and measurement simulation of a new digital receiver operating directly at millimeter-wave frequencies," *IEEE Transactions on Microwave Theory and Techniques*, vol. 43, no. 12, pp. 2766–2772, 1995.

[8] S. O. Tatu, E. Moldovan, K. Wu, and R. G. Bosisio, "A new direct millimeter-wave six-port receiver," *IEEE Transactions on Microwave Theory and Techniques*, vol. 49, no. 12, pp. 2517–2522, 2001.

[9] T. Hentschel, "The six-port as a communications receiver," *IEEE Transactions on Microwave Theory and Techniques*, vol. 53, no. 3, pp. 1039–1047, 2005.

[10] M. Mailand, R. Richter, and H.-J. Jentschel, "The influence of the rectified wave on the usability of six-port-based mobile receivers," in *Proceedings of the International Conference on Wireless and Mobile Communications (ICWMC '06)*, Bucharest, Romania, July 2006.

[11] H. S. Lim, W. K. Kim, J. W. Yu, H. C. Park, W. J. Byun, and M. S. Song, "Compact six-port transceiver for time-division duplex systems," *IEEE Microwave and Wireless Components Letters*, vol. 17, no. 5, pp. 394–396, 2007.

[12] S. M. Winter, H. J. Ehm, A. Koelpin, and R. Weigel, "Six-port receiver local oscillator power selection for maximum output SNR," in *Proceedings of the IEEE Radio and Wireless Symposium (RWS '08)*, pp. 151–154, Orlando, Fla, USA, January 2008.

[13] J. Östh, A. Serban, O. Owais et al., "Six-port gigabit demodulator," *IEEE Transactions on Microwave Theory and Techniques*, vol. 59, no. 1, pp. 125–131, 2011.

[14] E. E. Djoumessi, S. O. Tatu, and K. Wu, "Frequency-agile dual-band direct conversion receiver for cognitive radio systems,"

IEEE Transactions on Microwave Theory and Techniques, vol. 58, no. 1, pp. 87–94, 2010.

[15] A. Koelpin, G. Vinci, B. Laemmle, D. Kissinger, and R. Weigel, "The six-port in modern society," *IEEE Microwave Magazine*, vol. 11, no. 7, pp. S35–S43, 2010.

[16] A. Moscoso-Martir, I. Molina-Fernandez, and A. Ortega-Moñux, "Signal constellation distortion and BER degradation due to hardware impairments in six-port receivers with analog I/Q generation," *Progress in Electromagnetics Research*, vol. 121, pp. 225–247, 2011.

[17] C. de la Morena-Álvarez Palencia and M. Burgos-García, "Four-octave six-port receiver and its calibration for broadband communications and software defined radios," *Progress in Electromagnetics Research*, vol. 116, pp. 1–21, 2011.

[18] M. Bao, J. Chen, and L. Aspemyr, "A single-chip 15 to 30 GHz six-port demodulator for multi-Gb/s communication," in *Proceedings of the IEEE MTT-S International Microwave Symposium Digest (MTT '12)*, pp. 1–3, Montreal, Canada, June 2012.

[19] I. Molina-Fernandez, A. Moscoso-Martir, J. M. Avila-Ruiz et al., "Multi-port technology for microwave and optical communications," in *Proceedings of the IEEE MTT-S International Microwave Symposium Digest (MTT '12)*, pp. 1–3, Montreal, Canada, June 2012.

[20] B. Laemmle, K. Schmalz, J. Borngraeber et al., "A fully integrated 120-GHz six-port receiver front-end in a 130-nm SiGe BiCMOS technology," in *Proceedings of the IEEE 13th Topical Meeting on Silicon Monolithic Integrated Circuits in RF Systems (SiRF '13)*, pp. 129–131, 2013.

[21] G. Neveux, B. Huyart, and G. J. Rodriguez-Guisantes, "Wideband RF receiver using the "five-port" technology," *IEEE Transactions on Vehicular Technology*, vol. 53, no. 5, pp. 1441–1451, 2004.

[22] F. R. de Sousa and B. Huyart, "A 1.8—5.5 GHz integrated five-port front-end for wideband transceivers," in *Proceedings of the 7th European Conference on Wireless Technology (ECWT '04)*, pp. 67–69, October 2004.

[23] C. Mohamed, A. Khy, and B. Huyart, "A 1—20 GHz broadband MMIC demodulator for low if receivers in multistandard applications," *IEEE Transactions on Microwave Theory and Techniques*, vol. 57, no. 10, pp. 2318–2328, 2009.

[24] P. Pérez-Lara, I. Molina-Fernández, J. G. Wanguemert-Pérez, and A. Rueda-Pérez, "Broadband five-port direct receiver based on low-pass and high-pass phase shifters," *IEEE Transactions on Microwave Theory and Techniques*, vol. 58, no. 4, pp. 849–853, 2010.

[25] R. Mirzavand, A. Mohammadi, and F. M. Ghannouchi, "Five-port microwave receiver architectures and applications," *IEEE Communications Magazine*, vol. 48, no. 6, pp. 30–36, 2010.

[26] C. de la Morena-Alvarez-Palencia, K. Mabrouk, B. Huyart, A. Mbaye, and M. Burgos-Garcia, "Direct baseband I-Q regeneration method for five-port receivers improving DC-offset and second-order intermodulation distortion rejection," *IEEE Transactions on Microwave Theory and Techniques*, vol. 60, no. 8, pp. 2634–2643, 2012.

[27] K. Mabrouk and B. Huyart, "Circuit Analogique Pour le Calibrage Large Bande, la Suppression des Tensions Parasites dues aux DC-Offset et Produits d'Intermodulation IMD2 et Réduction d'un Convertisseur CAN Pour les Démodulateurs Zéro-IF ou Low-IF de Type Cinq-Port et Triphasé," Patent FR2934934 (A1), 2012.

[28] A. Khy and B. Huyart, "A 0.6—3. 6 GHz CMOS wideband demodulator for 4G mobile handsets," in *Proceedings of the European Microwave Integrated Circuits Conference*, pp. 560–563, 2012.

[29] B. Razavi, "Design considerations for direct-conversion receivers," *IEEE Transactions on Circuits and Systems II*, vol. 44, no. 6, pp. 428–435, 1997.

[30] G. Neveux, B. Huyart, and J. Rodriguez Guisantes, "Noise figure of a five-port system," in *Proceedings of the European Conference on Wireless Technology (ECWT '02)*, 2002.

[31] K. Mabrouk, F. R. de Sousa, B. Huyart, and G. Neveux, "Architectural solution for second-order intermodulation intercept point improvement in direct down-conversion receivers," *IET Microwaves, Antennas and Propagation*, vol. 4, no. 9, pp. 1377–1386, 2010.

[32] A. Kaissoine, B. Huyart, A. Mbaye, and K. Mabrouk, "Demodulation of aggregated RF signals with a unique Rx chain," in *Proceedings of New Circuits and Systems (NEWCAS '13)*, pp. 1–4, Paris, France, June 2013.

[33] A. Kaissoine, B. Huyart, and K. Mabrouk, "Demodulation of aggregated RF signals in three frequencies bands with a unique Rx chain," in *Proceedings of the European Microwave Conference*, pp. 561–564, Nuremberg, Germany, October 2013.